Int. J. Heat Mass Transfer. Vol. 15, pp. 217–233. Pergamon Press 1972. Printed in Great Britain

LAMINAR FILMWISE CONDENSATION ON A VERTICAL SURFACE

TETSU FUJII and HARUO UEHARA
Research Institute of Industrial Science, Kyūshū University, Fukuoka, Japan

(*Received* 22 *June* 1970)

Abstract—Two-phase boundary layer equations of laminar filmwise condensation are solved with an approximate method due to Jacobs under the conditions as follows; saturated vapour flows vertically downwards, a cooled surface of uniform temperature is placed parallel to the flow direction, both body force and forced convection are considered in the condensate film, which is so thin that the inertia and convection terms can be neglected. Numerical results for average coefficients of heat transfer are expressed as,

$$Nu_m = \left\{0{\cdot}656\left(1{\cdot}20 + \frac{1}{RH}\right)^{\frac{3}{4}} Re_l^2 + 0{\cdot}790\frac{Gr_l}{H}\right\}^{\frac{1}{2}}.$$

This expression is compared with experimental results hitherto reported. The agreement is fairly good for the cases where the temperature differences between the vapour and the cooled surface are restricted within some limitations and where Nu_m is smaller than 2×10^4. When the predicted Nu_m is larger than 2×10^4, the experimental Nu_m is about from 1·3 to 1·9 times as large as the predicted one except for the cases of small heat flux. The experimental data beyond the limitations of the temperature differences for organic substances show higher values of similar order at the smaller predicted Nu_m. The cause of these high values seems due to turbulence in the liquid film.

NOMENCLATURE

$A, B,$ coefficients in (26) and (27) or (36) and (37);
$c_p,$ specific heat at constant pressure;
$D,$ inner diameter of a cylinder;
$g,$ gravitational acceleration;
$Gr,$ Grashof number defined by (32) or (33);
$H,$ nondimensional number of condensation defined by (4);
$K,$ nondimensional number defined by (53);
$L,$ latent heat of condensation;
$l,$ height of a cooled surface;
$Nu,$ Nusselt number defined by (22) or (24);
$Nu^*,$ condensation number defined by (57);
$Pr,$ Prandtl number;
$q,$ heat flux;
$R,$ $\rho\mu$-ratio defined by (20);
$Re,$ Reynolds number defined by (41) or (46);
$Re^*,$ film Reynolds number defined by (58);
$T_s,$ temperature of vapour;
$T_w,$ temperature of a cooled surface;
$U, V,$ x- and y-component of vapour velocity respectively;
$U_\infty,$ vapour velocity outside the boundary layer;
$U_{in}, U_{out},$ mean velocities of vapour at the inlet and outlet of a tube respectively;
$u, v,$ x- and y-component of the velocity of the condensate;
$u_1,$ nondimensional velocity defined by (50);
$x, y,$ coordinate variables shown in Fig. 1;

x_c, transition point defined by (54) or (56);
z, nondimensional length defined by (49).

Greek symbols

α, coefficient of heat transfer defined by (21) or (23);
Δ, thickness of the vapour layer;
δ, thickness of the liquid film;
δ_1, nondimensional thickness of the liquid film defined by (51);
ζ, variable transformed by (13);
λ, thermal conductivity;
μ, dynamic viscosity;
ν, kinematic viscosity;
ρ, density.

Subscripts

l, value at $x = l$;
m, value averaged over the cooled surface;
x, local value at x;
δ, value at the interface between vapour and liquid;
exp, experimental value;
th, theoretical value.

Physical properties with and without superscript $^-$ are for vapour and liquid respectively.

1. INTRODUCTION

SIMILARITY solutions of the two-phase boundary layer equations concerning laminar filmwise condensation on a vertical surface were obtained by Koh *et al.* [1] and Koh [2] for the cases of body force convection and forced convection respectively. These solutions enable us to appreciate several assumptions which had been adopted in conventional approximate treatment, and to exhibit the ranges of parameters in which these approximate results can be applied. The similarity solutions, however, are inconvenient practically, because they have been given only for some numbers of combination of nondimensional parameters Pr, R and H.

When the vapour space is narrow relatively to the cooled surface, the film of the condensate is affected by self-created forced convection of the vapour, because the liquid film inspires the vapour of equal mass flow rate as a whole during steady condensation. On the contrary, for condensation on a vertical plate placed in forced flow of vapour, the liquid film is affected by the self-inclusive body force as the thickness increases.

There is no similarity solution of these combined body force and forced convection. Shekriladze–Gomelauri [3] proposed unique approximate solutions for various cases of condensation, introducing an assumption that the local shearing stress at the interface of vapour and liquid is equal to the momentum given up by condensing vapour. The limitations of nondimensional parameters for their application, however, are uncertain. Jacobs [4] proposed an approximate integral method for the two-phase boundary layer equations, and showed some curves of numerical results, which agreed fairly well with his experimental results for Freon 113 at atmospheric pressure. This agreement is unsatisfactory yet as verification of the theory, because measurements of heat-transfer coefficients of condensation are subject to relatively large errors. First of all, the theory itself must be logically exact, but his solutions do not coincide with similarity solutions for both limit cases of body force convection only and forced convection only.

The object of this study is to derive correct solutions concerning the condensation on a vertical surface with the approximate method similar to Jacobs, and to propose simple expressions of the numerical results. Then a newly derived expression for the average coefficient of heat transfer is compared with experimental results hitherto reported.

2. BASIC EQUATIONS

In Table 1 are shown some rough values of principal parameters concerning filmwise condensation. Within respective limitations of temperature difference between the saturated vapour

Table 1. Examples of parameters Pr, R, H *and limitations of* $(T_s - T_w)$

	T (°C)	Pr	R	$\frac{H}{(T_s - T_w)} \times 10^3$ (1/deg)	$(T_s - T_w)_B$ (deg)	$(T_s - T_w)_F$ (deg)
Acetone	56·1	3	90	1	35	100
Benzene	80·1	5	120	1	20	15
Diphenyl	255·3	5	100	0·7	30	30
Ethanol	78·4	11	150	0·6	15	7
Methanol	64·5	5	180	1	20	6
Toluene	110·8	4	83	3	10	4
Water	20	5	2000	0·3	70	20
Water	100	2	200	1	50	50

T, saturation temperature.
$(T_s - T_w)_B$, limitation of temperature difference in (30) for body force convection.
$(T_s - T_w)_F$, limitation of temperature difference in (44) for forced convection.

and the cooled surface $(T_s - T_w)$ given in the Table, the approximate solutions of Nusselt [5] and Cess [6] are applicable to the cases of body force and forced convection respectively within the accuracy of a few per cent [1, 2]. These suggest that the inertia and convection terms in the boundary layer equations of the liquid film may be neglected prior to theoretical calculations. The variation of the physical properties with temperature for small temperature differences, vapour density relative to liquid density, and thermal resistance at vapour–liquid interface [8, 23] may be also neglected. Furthermore, it is assumed that the temperature of the cooled surface is uniform, the vapour is saturated, and the flows of both the vapour and the condensate are laminar.

Figure 1 shows the physical model and coordinate system. By means of the aforementioned assumptions, equations of continuity, momentum and energy are written simply as follows; for the liquid film,

$$\frac{\partial u}{\partial x} + \frac{\partial v}{\partial y} = 0, \tag{1}$$

$$\nu \frac{\partial^2 u}{\partial y^2} + g = 0, \tag{2}$$

$$\delta \frac{\mathrm{d}}{\mathrm{d}x} \int_0^\delta u \, \mathrm{d}y = \frac{\lambda (T_s - T_w)}{\rho L} \equiv \nu H \tag{3}$$

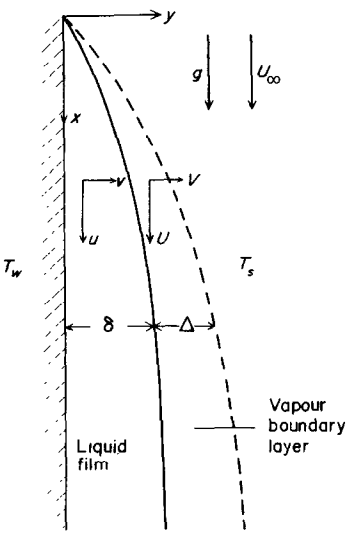

FIG. 1. Physical model and coordinate system.

where

$$H = \frac{c_p (T_s - T_w)}{PrL}, \tag{4}$$

for the vapour boundary layer,

$$\frac{\partial U}{\partial x} + \frac{\partial V}{\partial y} = 0, \tag{5}$$

$$\frac{\partial U^2}{\partial x} + \frac{\partial UV}{\partial y} = \bar{\nu} \frac{\partial^2 U}{\partial y^2}, \tag{6}$$

with the boundary conditions,

$$y = 0; \quad u = 0, \quad v = 0, \quad T = T_w, \tag{7}$$

$$\zeta = \Delta; \quad U = U_\infty, \quad \frac{\partial U}{\partial y} = 0, \quad T = T_s, \tag{8}$$

and with the compatibility conditions of velocity, shearing stress, condensation rate and temperature at the vapour–liquid interface respectively,

$$y = \delta \text{ or } \zeta = 0;$$

$$u_\delta = U_\delta, \tag{9}$$

$$\mu\left(\frac{\partial u}{\partial y}\right)_\delta = \bar{\mu}\left(\frac{\partial U}{\partial y}\right)_\delta, \tag{10}$$

$$\rho\frac{\mathrm{d}}{\mathrm{d}x}\left(\int_0^\delta u\mathrm{d}y\right) = \rho\left(u\frac{\mathrm{d}\delta}{\mathrm{d}x} - v\right)_\delta = \bar{\rho}\left(U\frac{\mathrm{d}\delta}{\mathrm{d}x} - V\right)_\delta, \tag{11}$$

$$T_\delta = T_s, \tag{12}$$

where

$$\zeta = y - \delta. \tag{13}$$

Integrating (2) twice subject to (7) and (9), we obtain

$$u = \left(\frac{u_\delta}{\delta} + \frac{g\delta}{2\nu}\right)y - \frac{g}{2\nu}y^2. \tag{14}$$

Substituting (14) into (3), we obtain

$$\nu H = \frac{\delta}{2}\frac{\mathrm{d}(u_\delta\delta)}{\mathrm{d}x} + \frac{g\delta^3}{4\nu}\frac{\mathrm{d}\delta}{\mathrm{d}x} \tag{15}$$

$$= \frac{\delta}{2}\frac{\mathrm{d}u_\delta}{\mathrm{d}x} + \left(\frac{u_\delta}{4} + \frac{g\delta^2}{8\nu}\right)\frac{\mathrm{d}\delta^2}{\mathrm{d}x}. \tag{15'}$$

When the velocity profile in the vapour layer is taken as a quadratic formula of ζ subject to (8) and (9), it is expressed as;

$$U = u_\delta + (U_\infty - u_\delta)\left(\frac{2\zeta}{\Delta} - \frac{\zeta^2}{\Delta^2}\right). \tag{16}$$

Integrating (5) and (6) from 0 to Δ with respect to ζ, and then eliminating V with (3) and (11), we obtain

$$\frac{\mathrm{d}}{\mathrm{d}x}\int_0^\Delta U(U_\infty - U)\,\mathrm{d}\zeta + \frac{\rho\nu H}{\bar{\rho}\delta}(U_\infty - u_\delta) = \bar{\nu}\left(\frac{\partial U}{\partial\zeta}\right)_{\tau=0}. \tag{17}$$

By substituting (14) and (16) into (10), the ratio of the thickness of both layers is given as

$$\frac{\Delta}{\delta} = \frac{2\bar{\mu}(U_\infty - u_\delta)}{\mu(u_\delta - g\delta^2/2\nu)}. \tag{18}$$

Substituting (16) into (17) and eliminating Δ with (18), we obtain,

$$\frac{\mathrm{d}}{\mathrm{d}x}\left\{\frac{(U_\infty - u_\delta)^2(2U_\infty + 3u_\delta)\delta}{(u_\delta - g\delta^2/2\nu)}\right\} + \frac{15R^2\nu(U_\infty - u_\delta)}{2\delta}\left\{H - \frac{u_\delta - g\delta^2/2\nu}{U_\infty - u_\delta}\right\} = 0, \tag{19}$$

or

$$\frac{\{-2(U_\infty^2 + U_\infty^2 u_\delta + 3u_\delta^2) + (U_\infty + 9u_\delta)\}\delta^2}{(u_\delta - g\delta^2/2\nu)^2}\frac{\mathrm{d}u_\delta}{\mathrm{d}x} + \frac{(U_\infty - u_\delta)(2U_\infty + 3u_\delta)(u_\delta + g\delta^2/2\nu)}{2(u_\delta - g\delta^2/2\nu)^2}\frac{\mathrm{d}\delta^2}{\mathrm{d}x} + \frac{15R^2\nu}{2}\left\{H - \frac{u_\delta - g\delta^2/2\nu}{U_\infty - u_\delta}\right\} = 0, \tag{19'}$$

where

$$R = (\rho\mu/\bar{\rho}\bar{\mu})^{\frac{1}{4}}. \tag{20}$$

If u_δ and δ are solved simultaneously from (15) and (19), the local coefficient of heat transfer, the local Nusselt number, the average coefficients of heat transfer and the average Nusselt number are given by the following formula respectively,

$$\alpha_x = \frac{q}{(T_s - T_w)} = \frac{\lambda}{\delta}, \tag{21}$$

$$Nu_x = \frac{\alpha_x x}{\lambda} = \frac{x}{\delta}, \tag{22}$$

$$\alpha_m = \frac{1}{(T_s - T_w)\,l}\int_0^l q\,\mathrm{d}x, \tag{23}$$

$$Nu_m = \frac{\alpha_m l}{\lambda}. \tag{24}$$

3. NUMERICAL RESULTS AND THEIR APPROXIMATE EXPRESSIONS

3.1 *Case of body force convection*

For the case that $U_\infty = 0$, (19) reduces to

$$\frac{\mathrm{d}}{\mathrm{d}x}\left(\frac{3u_\delta^2\delta}{u_\delta - g\delta^2/2\nu}\right) - \frac{15R^2\nu u_\delta}{2\delta} \times\left(H - \frac{u_\delta - g\delta^2/2\nu}{u_\delta}\right) = 0. \tag{25}$$

The simultaneous equations (15) and (25) take the following particular solutions,

$$u_\delta = \frac{A}{2}(gHx)^{\frac{1}{2}}, \quad \delta = B\left(\frac{\nu^2 Hx}{g}\right)^{\frac{1}{4}}, \tag{26),(27}$$

where the coefficients A and B are solved from the following equations, which are derived by substituting (26) and (27) into (15) and (25)

$$B^4 + 3AB^2 - 16 = 0, \tag{28}$$

$$A^3B^2 + 4R^2A(B^2 - A) - \frac{4R^2}{H}(B^2 - A)^2 = 0. \tag{29}$$

Since R^2/H is much larger than unity in reality, (29) is approximated as $B^2 - A \approx 0$. It is therefore obtained that

$$A = 2 \quad \text{and} \quad B = \sqrt{2}.$$

The local and average Nusselt number are expressed respectively as;

$$Nu_x = \frac{1}{B}\left(\frac{x^3 g}{\nu^2 H}\right)^{\frac{1}{4}} \approx \left(\frac{Gr_x}{4H}\right)^{\frac{1}{4}}, \tag{30}$$

$$Nu_m = \frac{4}{3}\left(\frac{Gr_l}{4H}\right)^{\frac{1}{4}}, \tag{31}$$

where

$$Gr_x = \frac{x^3 g}{\nu^2} \quad \text{and} \quad Gr_l = \frac{l^3 g}{\nu^2}. \tag{32),(33}$$

These results correspond to the Nusselt's [5]. By the way only one pair, which satisfies the conditions $B^2 > A > 0$ and $B > \sqrt{2}$, among the six pairs of roots of (28) and (29), has physical meaning, because Δ must be positive.

3.2 *Case of forced convection*

For the case that $g = 0$, (15) and (19) reduce respectively to

$$\nu H = \frac{\delta}{2}\frac{\mathrm{d}(u_\delta\delta)}{\mathrm{d}x}, \tag{34}$$

$$\frac{\mathrm{d}}{\mathrm{d}x}\left\{\frac{(U_\infty - u_\delta)^2(2U_\infty + 3u_\delta)\,\delta}{u_\delta}\right\} + \frac{15R^2\nu(U_\infty - u_\delta)}{2\delta}\left\{H - \frac{u_\delta}{U_\infty - u_\delta}\right\} = 0. \tag{35}$$

The particular solutions of these simultaneous equations are

$$u_\delta = AU_\infty, \quad \delta^2 = Bx, \tag{36),(37}$$

where the coefficients A and B are solved from the following equations

$$B = \frac{4\nu H}{AU_\infty}, \tag{38}$$

$$\frac{4(1 - A)^2(2 + 3A)}{R^2} - \frac{15A^3}{H} + 15(1 - A)A^2 = 0. \tag{39}$$

The local Nusselt number is expressed as,

$$Nu_x = (\sqrt{A})\left(\frac{U_\infty x}{4\nu H}\right)^{\frac{1}{4}} = \frac{(\sqrt{A})(\sqrt{Re_x})}{2\sqrt{H}}, \tag{40}$$

where

$$Re_x = \frac{U_\infty x}{\nu}. \tag{41}$$

Numerical results are shown in the relation

of $Nu_x/\sqrt{Re_x}$ vs. RH in Fig. 2. Because these results have the characteristics as,

for $RH \ll 1$, $Nu_x/(\sqrt{Re_x}) = 0{\cdot}450\,(RH)^{-\frac{1}{4}}$, (42)

for $RH \to 10$, $Nu_x/(\sqrt{Re_x}) = 0{\cdot}500$, (43)

in the range of $RH < 10$, it may be proposed that

$$\frac{Nu_x}{\sqrt{Re_x}} = 0{\cdot}450\left(1{\cdot}20 + \frac{1}{RH}\right)^{\frac{1}{4}}. \tag{44}$$

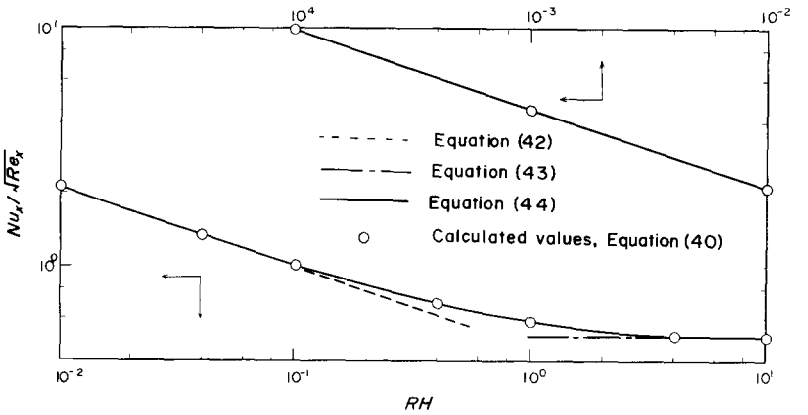

FIG. 2. Local coefficients of heat transfer in forced convection.

This expression agrees with the numerical results and with Cess' approximate solutions [6] within the errors of maximum 2 per cent and about three per cent respectively.

The average Nusselt number is expressed as

$$\frac{Nu_m}{\sqrt{Re_l}} = 0{\cdot}90\left(1{\cdot}20 + \frac{1}{RH}\right)^{\frac{1}{4}}, \tag{45}$$

where

$$Re = U_\infty l/\nu. \tag{46}$$

3.3 *Case of combined body force and forced convection*

The simultaneous equations (15)′ and (19)′ are nondimensionalized respectively such that by using the following formula

$$z = \frac{gx}{U_\infty^2}, \quad u_1 = \frac{u}{U_\infty}, \tag{49), (50}$$

$$\delta_1^2 = \delta^2\left(\frac{g}{\nu U_\infty}\right). \tag{51}$$

Because $\delta_1 = 0$ at $z = 0$ physically, (47) and (48) cannot but be solved with power series expansion method in the range of small z, that is, the formula

$$u_{1\delta} = A_0 + A_1 z + \ldots,$$

$$\delta_1^2 = B_1 z + B_2 z^2 + \ldots$$

are substituted into (47) and (48), then coefficients of the terms with same power of z are taken as

$$\frac{\delta_1^2}{2}\frac{du_{1\delta}}{dz} + \left(\frac{u_{1\delta}}{4} + \frac{\delta_1^2}{8}\right)\frac{d\delta_1^2}{dz} = H. \tag{47}$$

$$\frac{\left\{-2(1 + u_{1\delta} + 3u_{1\delta}^2) + (1 + 9u_{1\delta})\dfrac{\delta_1^2}{2}\right\}\delta_1^2}{(u_{1\delta} - \delta_1^2/2)^2}\frac{du_{1\delta}}{dz}$$

$$+ \frac{(1 - u_{1\delta})(2 + 3u_{1\delta})(u_{1\delta} + \delta_1^2/2)}{2(u_{1\delta} - \delta_1^2/2)^2}\frac{d\delta_1^2}{dz}$$

$$+ \frac{15R^2}{2}\left\{H - \frac{u_{1\delta} - \delta_1^2/2}{1 - u_{1\delta}}\right\} = 0, \tag{48}$$

zero identically. Thus derived equations of A_0 and B_1 take the same form as (38) and (39). This fact indicates that the liquid film near the leading edge is unaffected by body force. In the range $z < 10^{-5}$ the solutions in previous item 3.2 were employed, and in the range $z > 10^{-5}$ (47) and (48) were integrated successively with Runge–Kutta–Gill method.

The numerical results for four combinations of R, H are shown in the relation of $Nu_x/\sqrt{Re_x}$ vs. z/H in Fig. 3. The values at small z/H in this

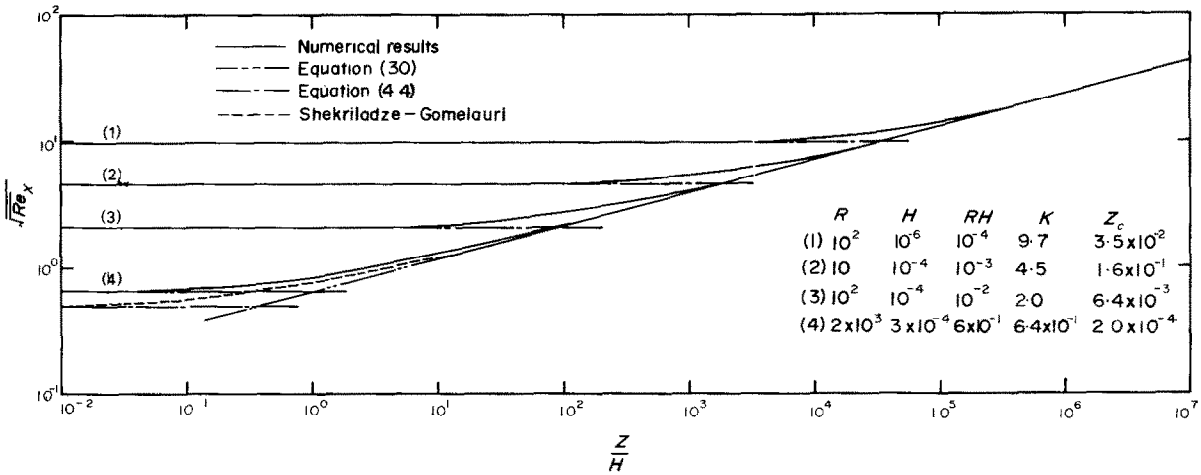

FIG. 3. Local coefficients of heat transfer in combined convection.

figure is naturally coincident with those of the same RH in Fig. 2. With increasing of z each curve transits gradually to a curve, which exhibits the characteristic of the body force convection. An approximate expression, therefore, may be proposed such that

$$\frac{Nu_x}{\sqrt{Re_x}} = K\left\{1 + \frac{1}{4K^4}\frac{z}{H}\right\}^{\frac{1}{4}}, \tag{52}$$

where

$$K = 0{\cdot}450\left(1{\cdot}20 + \frac{1}{RH}\right)^{\frac{1}{4}}. \tag{53}$$

The maximum discrepancy between the numerical results and this expression is only 2·5 per cent.

The cross points of the curves of (30) and (44) shown in Fig. 3 yield the expression

$$x_c = \frac{4K^2U_\infty^2 H}{g}. \tag{54}$$

It may be considered roughly that x_c is a transition point from the region of forced convection dominance to that of body force one.

The solution of Shekriladze–Gomelauri [3] is expressed by using the nondimensional parameter in this paper as;

$$\frac{Nu_x}{\sqrt{Re_x}} = \frac{1}{2}\left\{\frac{1}{2} + \left(\frac{1}{4} + \frac{4z}{H}\right)^{\frac{1}{4}}\right\}^{\frac{1}{4}}.$$

It is clarified numerically that this expression corresponds to (52) at $RH \approx 10$ as shown in Fig. 3. Since Jacobs [4] gave $V = 0$ instead of $\partial U/\partial y = 0$ in the boundary condition (8),

additional parameters $\rho/\bar{\rho}$ and $\nu/\bar{\nu}$ emerged in the subsequent equations. These are unreasonable.

The average coefficients of heat transfer are obtained by integrating (52) with respect to x. Some results by Simpson's integration rule are shown in Fig. 4. An expression that satisfies the characteristics of both limit cases of body force only and forced convection only, may be proposed as

$$\frac{Nu_m}{\sqrt{Re_l}} = 2K\left\{1 + \left(\frac{\sqrt{2}}{3K}\right)^4 \frac{z_l}{H}\right\}^{\frac{1}{4}},$$

or (55)

$$Nu_m = \left\{0{\cdot}656\left(1{\cdot}20 + \frac{1}{RH}\right)^{\frac{3}{4}} Re_l^2 + 0{\cdot}790\frac{Gr_l}{H}\right\}^{\frac{1}{4}}.$$

4. COMPARISON WITH EXPERIMENTAL RESULTS

The theoretical results obtained in the previous section are compared with experimental results hitherto reported on average coefficients of heat transfer. Many experiments concerning the condensation on a vertical surface were performed with the inner surface of a tube from practical interest, while some were with a plate or the outer surface of a cylinder mainly from theoretical interest. In Table 2 are listed up the experiments, in the data of which the vapour velocities are represented or can be calculated, including the cases where the velocities may be appreciated to be zero.

The rearranged data are plotted in Figs. 5 and 6, respectively for water and organic substances, the ordinate of which is measured Nusselt number $(Nu_m)_{exp}$ and the abscissa is predicted one $(Nu_m)_{th}$ from (55). The calculation

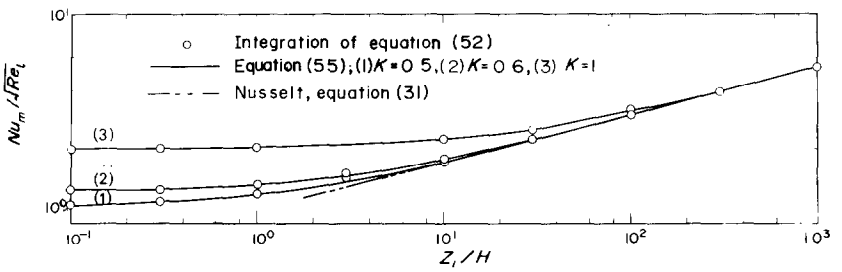

FIG. 4. Average coefficients of heat transfer in combined convection.

This expression agrees with each integrated value within the accuracy of about four per cent. By the way, the transition point from forced convection to body force one in (55) is evaluated approximately as;

$$(x_c)_m = \frac{20K^4U_\infty^2 H}{g}. \quad (56)$$

The effect of forced convection is apparently broadened for the average coefficients of heat transfer.

of the nondimensional numbers in (55) was performed under the following rules;

(i) As the representative temperature of the cooled surface T_w, is adopted the value at the middle height of the surface, as far as the temperature distribution is available. In most data, however, merely the mean values are represented.

(ii) As the representative velocity of vapor is adopted the value at the inlet portion or at the leading edge. This choice is based on somewhat practical convenience, therefore, detailed theoretical consideration remains to be required.

When the vapour velocities are not described in the literature, they are evaluated such that the total condensation rates are divided by the cross sectional area of the vapour path and by the density of the vapour at the inlet portion.

(iii) As physical properties of the liquid film are adopted the values at reference temperature $T_r = T_w + 0{\cdot}3\,(T_s - T_w)$, which is referred from the theoretical results of Poots–Milles [7].

4.1 *Cases of water*

In the first place, there are treated the cases where the body force convection is dominant, that is, where the transition height $(x_c)_m$ shown in Table 2 is much smaller than the total height of the cooled surface. Mills–Seban, cf. Table 3 of [8], as to a small plate of about 0·127 m height placed in relatively large space of steam at about 0·01 ata, showed that the thermal resistance at the interface of vapour and liquid film was negligibly small, as well as Nusselt's prediction (31) was consistent. Burov, cf. Figs. 3–5 of [9], as to the outer surfaces of cylinders of 1, 0·55 and 0·275 m height placed in relatively large space of steam at about atmospheric pressure, found that the values of $(Nu_m)_{exp}$ were about 10 per cent larger than those predicted by (31). Hebbard–Badger, cf. Table 1 of

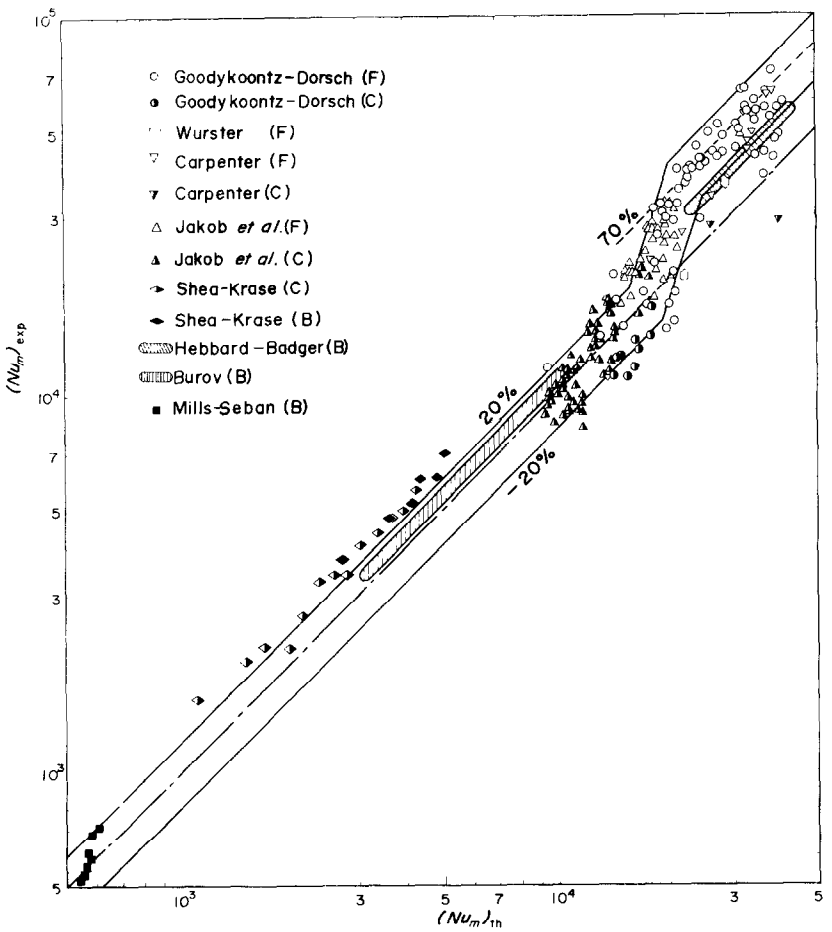

FIG. 5. Correlation between experimental $(Nu_m)_{exp}$ and theoretical $(Nu_m)_{th}$ predicted from (55) for water.

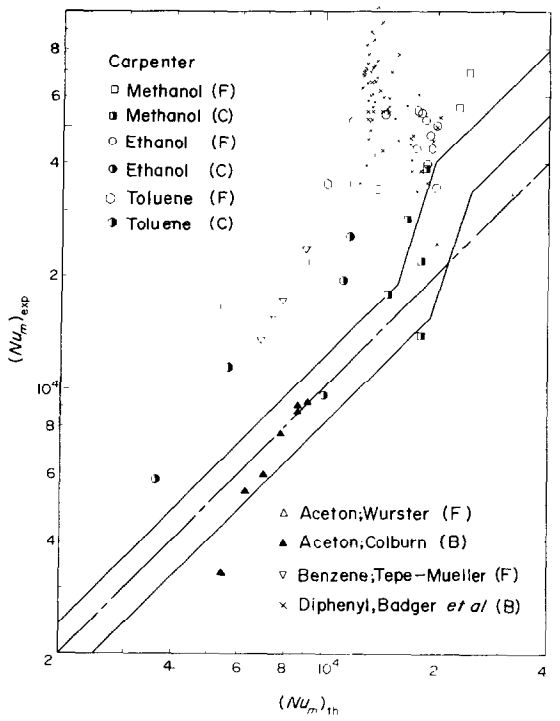

FIG. 6. Correlation between experimental $(Nu_m)_{exp}$ and theoretical $(Nu_m)_{th}$ predicted from (55) for organic substances.

[10], as to the outer surface of a tall cylinder of 3·6 m height, found that the values of $(Nu_m)_{exp}$ were about 34 per cent larger than those predicted by (31).

Shea–Krase, cf. Table 2 and Fig. 6 of [11], measured local coefficients of heat transfer by dividing a plate of 0·584 m height vertically into five heat transferring sections, and showed that the steam velocity made the coefficients large from 9 to 18 per cent, when x_c was from 0·003 to 0·016 m. With regard to the data rearranged in Fig. 5, the coefficients of heat transfer are averaged from the top to the corresponding section, and the symbols of body force convection and combined convection are corresponding to the cases where $(x_c)_m/l$ is smaller and larger than 0·1 respectively. Because the effects of both the vapour velocity and the representative temperature difference are taken into account, the scattering of the data is diminished to the extent of the same order as the measurement error. On the whole, however, the experimental values are larger than those predicted by (55). The cause seems due to the clumsy estimation of the heat flux, since the temperature rise of cooling water is very small.

Goodykoontz–Dorsh performed various and careful measurements and demonstrated the detailed data, which pertained to the inner surfaces of a steel tube of 0·0159 m i.d. and 2·44 m length, cf. Table 1 of [12], and of a copper tube of 0·00745 m i.d. and the same length, cf. Table 1 of [13]. The former data cover the cases of both combined and forced convection, while the latter mainly of the forced convection. Since steam has completely condensed in the tube, the effective length of heat transfer is different in every run. For the data in the range of $(Nu_m)_{th} < 2 \times 10^4$, rearranged in Fig. 5, the values of $(Nu_m)_{exp}$ are about 20 per cent smaller than those of $(Nu_m)_{th}$ for the former experiments, on the other hand about 20 per cent larger for the latter experiments, though the scattering of respective data is appreciated to be about 10 per cent. These discrepancies seem due to experimental error peculiar to respective apparatus. In the range of $(Nu_m)_{th} > 2 \times 10^4$, most of the data are located on a line which lies about 70 per cent higher than theoretically predicted one, however, some are lower than the curve. These $(Nu_m)_{exp}$ are evaluated apparently lower, because the saturation temperature corresponding to the static pressure at the inlet portion is taken as the representative one, although the static pressures of the steam vary remarkably towards the flow direction.

Carpenter, cf. Table IV of [14], experimented with the inner surface of a tube of 0·01165 m i.d. and 2·53 m length. Some data pertain to the case where steam has completely condensed in the tube, and others to the case where steam flows through the tube. Carpenter represented average values of overall heat transfer coefficients, overall temperature difference and heat transfer coefficients of steam side without

Table 2. Data referred in Figs. 5 and 6

	Substance	T_s (°C)	T_w (°C)	Pr	H $\times 10^2$	RH	Cooled surface	l (m)	U_∞ (m/s)	$(x_c)_m$ (m)	Convection pattern
Hebbard–Badger [10]	water	80–120	73–114	1·4–1·9	0·5–1·4	0·9–2·2	OSC	3·66	0·05	0·002	B
Jakob *et al.* [15]	water	100	71–96	1·9–2·2	0·5–2·7	0·2–9·0	ISC	1·2	10–80	0·14–83	C, F
Shea–Krase [11]	water	100	45–83	1·9–2·5	1·7–3·5	4·2–13·0	FP	0·584	1·4–3·7	0·017–0·062	B, C
Wurster [20]	water	100	28	3	3·8	10·3	ISC	4·36	74	24<	F
								3·63	104		
Carpenter [14]	water	100–108	74–96	1·8–2·1	0·4–2·4	0·5–0·8	ISC	1·2–2·5	27–174	0·38–37	C, F
Burov [9]	water	101	82–95	1·9	0·6–1·8	1·4–4·4	OSC	1·0–0·275	0·5	0·0003	B
Goodykoontz–Dorsch [12]	water	102–134	67–100	1·6–2·2	2·3–5·3	4·0–6·8	ISC	2·44	20–70	0·34–3·7	C, F
Goodykoontz–Dorsch [13]	water	98–129	67–97	1·8–2·2	1·9–5·1	3·0–7·8	ISC	2·44	95–310	48–530	F
Mills–Seban [8]	water	7–10	5	12	0·075	3·6	FP	0·127	0	0	B
Badger *et al.* [22]	diphenyl	260–293	210–240	4–6	1·5–8·0	1·1–7·0	OSC	3·66	1–15	<0·008	B
Colburn *et al.* [20]	acetone	56·1	42–51	3·1	0·7–1·8	0·6–1·8	ISC	0·971	2·5–5·8	0·014–0·1	B
Wurster [20]	acetone	56·1	34·6	3·4	2·6	2·0	ISC	4·77	48·7	10·5	F
Tepe–Mueller [21]	benzene	80·1	41–48	3·3	2·7–3·3	3·9–4·7	ISC	0·915	20–41	1·8<	F
Carpenter [14]	ethanol	78–82	43–66	11–12	0·3–1·1	0·5–1·7	ISC	0·32–2·53	2·6–74	0·002–15	C, F
	methanol	65–71	43–53	5·1–5·4	0·6–1·3	0·9–1·7	ISC	2·31–2·53	19–93	0·65–20	C, F
	toluene	111–117	74–95	3·8–4·1	2·5–5·3	2·0–4·5	ISC	0·49–2·53	11–48	0·69–14	C, F

In the column of cooled surface: FP, flat plate; ISC, inner surface of a cylinder; OSC, outer surface of a cylinder. In the column of convection pattern: B, body force convection; C, combined convection; F, forced convection.

measuring wall temperature. Since steam temperature falls gradually towards flow direction except near the inlet portion as shown in one example in [14], the experimental data rearranged in Fig. 5 are calculated with the assumed values of T_w such that $T_w = (T_s)_{out} - (T_s - T_w)_m$, where $(T_s)_{out}$ is steam temperature measured at the bottom and $(T_s - T_w)_m$ is average temperature difference between steam and wall calculated from the original table. The general characteristics of correlation in Fig. 5 are similar to those of Goodykoonts–Dorsch, except for two points of combined convection, which are corresponding to the case of very small rates of condensation.

In the experiments by Jakob *et al.*, cf. Fig. 12 of [15], steam flows through a tube of 0·04 m i.d. and 1·21 m length. The data for the cases where the steam velocities at the inlet are about 10–40 m/s and 60–80 m/s, are corresponding to the combined convection and the forced one respectively. Most of the data rearranged in Fig. 5 are in good agreement with the theoretical prediction within the accuracy of measurements. Some data with vapour velocity of 80 m/s, $(Nu_m)_{th}$ of which is at about 2×10^4, are as large as those of Goodykoontz–Dorsch than the theoretical predictions.

Wurster, cf. Table 1 of the discussion of [20], calculated the average coefficients of heat transfer in commercial condensers. The data, appreciated as forced convection, are in fairly good agreement with the theoretical predictions.

In the range of $(Nu_m)_{th} < 2 \times 10^4$, expression (55) with the effects of both vapour velocity and body force correlates adequately the experimental data on any cases of a vertical plate and the inner and outer surface of a vertical cylinder, though the conditions of the experiments are not strictly coincident with the theoretical assumptions, especially as to the distribution of the surface temperature, the variation of vapour velocity and the flow regime of the vapour, namely, laminar or turbulent. In the range of $(Nu_m)_{th} > 2 \times 10^4$, however, the most data are distributed between 30 and 90 per cent larger values than the theoretical predictions. The cause of these larger values seems due to turbulence induced in the liquid film. A best fitted band with 20 per cent width for the experimental results is shown in Fig. 5.

By the way, it must be noted that the predicted values of the average Nusselt number $(Nu_m)_{th}$ are widely affected by the choice of the representative values of the surface temperature, vapour temperature and vapour velocity. The physical properties in the rearrangement of this section are referred from [16].

4.2 *Cases of organic substances*

All the experimental results in Table 2 except for water are rearranged with respective symbols in Fig. 6. Though some of the physical properties are altered by referring to [17–19], their values especially for thermal conductivity are somewhat uncertain yet. Therefore, the nondimensional data of these substances contain perhaps larger errors than those of water.

The best fitted band obtained for water is also inserted in Fig. 6. Most points for methanol and three points for ethanol by Carpenter, cf. Table IV of [14], and most points for aceton by Colburn *et al.*, cf. Table 1 of [20], are distributed within the band or very near it. The lowest point for the latter experiments is somewhat uncertain, because the total length of the tube is taken as the effective length of heat transfer commonly. The value evaluated from a commercial condenser of aceton by Wurster, cf. Table 1 of the discussion of [20], is in good agreement with that predicted from (55) though $(Nu_m)_{th}$ is larger than 2×10^4. The flow of liquid film in this case seems to be laminar owing to relatively small heat flux. The temperature differences $(T_s - T_w)$ of all above data are taken within the respective limitations given in Table 1.

The values of $(Nu_m)_{exp}$ for the other data, together with toluene by Carpenter [20], benzen by Tepe–Mueller, cf. Table 1 of [21], and diphenyl by Badger *et al.*, cf. Tables I and II of [22], are about from 2 to 10 times as large

as $(Nu_m)_{th}$, and the values of $(T_s - T_w)$ are beyond the respective limitations. The similarity solutions [1, 2] suggest that the data of these conditions of temperature differences take somewhat larger values than those predicted by (55). It is reasonable to consider that these effects due to convection terms will become more emphasized, when the flow of the liquid film becomes turbulent.

For very small $(Nu_m)_{th}$ of body force convection, by the way, Slegers–Seban [23] obtained the same results with n-butyl alcohol as Mills–Seban [8] with water.

5. REMARKS ON THE NONDIMENSIONAL EXPRESSION OF HEAT TRANSFER COEFFICIENTS BY MEANS OF FILM REYNOLDS NUMBER

Experimental data on the heat transfer coefficients of condensation in a circular or annular tube are usually correlated in the relation between condensation number Nu^* and film Reynolds number Re^*, which are defined respectively by

$$Nu^* = \frac{\alpha_m}{\lambda}\left(\frac{\nu^2}{g}\right)^{\frac{1}{3}}, \quad Re^* = \frac{4lq_m}{\mu L}. \qquad (57), (58)$$

In Fig. 7 data on diphenyl by Badger *et al.* [22, 24] and on water by Carpenter–Colburn [14, 25] and by Goodykoontz–Dorsch [12] are referred from the corresponding figure of each literature. For the first time, Kirkbride [26] proposed this kind of coordinates, by which the data of Badger *et al.* were correlated successfully. It has been considered, therefore, that the tendency that the values of Nu^* are separated with increasing Re^* from a curve corresponding to Nusselt's theory as shown in Fig. 7, indicates the existence of turbulent film. However, the widely scattered data such as shown in Fig. 7 make it impossible to predict the heat transfer coefficients for any condition of condensation.

When vapour condenses in a tube, the vapour velocity depends on the average heat flux, that is, the following relation is given,

$$U_{in} - U_{out} = \frac{4lq_m}{D\bar{\rho}L}, \qquad (59)$$

where U_{in} and U_{out} are the sectional mean vapour velocity at inlet and outlet respectively. If (55) is consistent, namely, the flow of the liquid film is laminar, mean heat flux q_m is calculated by

$$q_m = \frac{2\lambda K(T_s - T_w)}{l}\left\{1 + \left(\frac{\sqrt{2}}{3K}\right)^4 \frac{gl}{U_{in}^2 H}\right\}^{\frac{1}{4}} \times \left(\frac{U_{in} l}{\nu}\right)^{\frac{1}{4}}. \qquad (60)$$

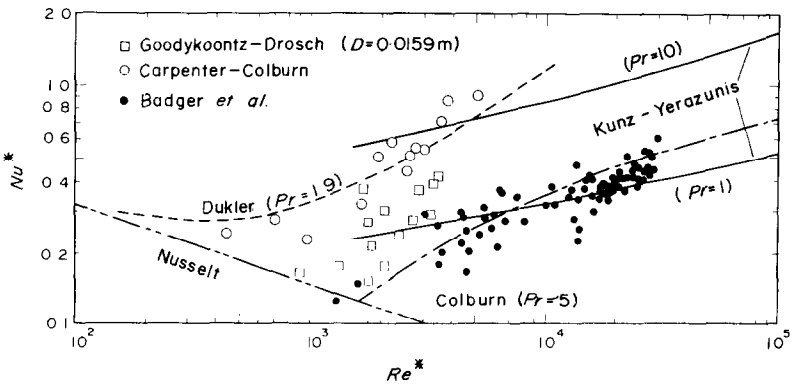

FIG. 7. Comparison between experiments and theoretical results hitherto reported in the relation of Nu^* vs. Re^*.

When $(T_s - T_w)$ and q_m are calculated from (59) and (60) numerically with a parameter $(U_{in} - U_{out})$, Nu^* and Re^* are evaluated from (57) and (58) respectively.

A comparison between experiments and theoretical calculations are shown in Fig. 8, where the nondimensional data are calculated from the original data of Goodykoontz–Dorsch

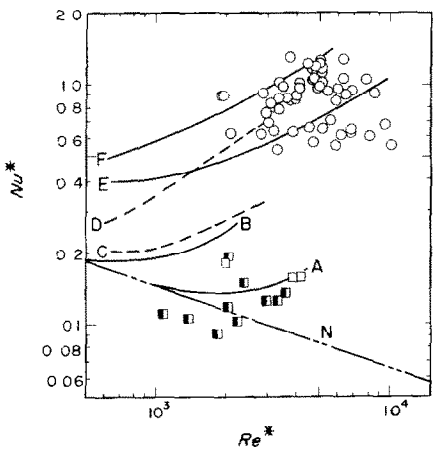

FIG. 8. Comparison between experimental data by Goodykoonts–Dorsch and Nu^* predicted by the authors.

	D (mm)	T_s (°C)	l (m)	
A	15·9	140	2	laminar
B	15·9	100	2	laminar
C	7·44	110	2	laminar
D	7·44	110	0·7	laminar
E	7·44	110	2	turbulent
F	7·44	110	0·7	turbulent
N	Nusselt's prediction			laminar

○ forced convection, D = 7·44 mm
□ forced convection, D = 15·9 mm
◧ combined convection, D = 15·9 mm

with the aforementioned rules and the representative conditions of the experiments shown in the table attached to the figure are taken as the conditions of the calculation. Furthermore, the curves E and F in the figure are obtained by using 1·7 q_m instead of q_m as examples for the case of turbulent film, though the characteristics of this case are not yet clarified. The correspondency between the experimental data and the calculated curves is in similar trend as in Fig. 5. The fact that the data for D = 0·0159 m of Goodykoontz–Dorsch in Figs. 7 and 8 are inconsistent with each other in spite of the same data, is mainly due to the different definitions of average coefficients of heat transfer, that is, those by Goodykoontz–Dorsch in Fig. 7 are average values of local heat transfer coefficients, while those by the authors in Fig. 8 are average values calculated by using representative temperature differences.

The demonstration in Fig. 8 allows the following conclusion. In the first place, the tendency, that the values of Nu^* separate from the Nusselt's prediction and increase more and more with increasing of Re^*, indicates a characteristic of the condensation in a tube, whether the flow of the liquid film is turbulent or not. In the second place, the calculated curves are remarkably affected by the diameter and effective length of the tube, vapour temperature and variation of the physical properties with temperature. Furthermore, when the condensation has not completed in the tube, the curves are also affected by the vapour velocity at the outlet U_{out}, though this effect is not shown in the figure. Inclusively, it is not adequate to use the relation of Nu^* vs. Re^* for the correlation of the heat transfer data on condensation in a tube, because the nondimensionalized data are affected by the dimensions of the apparatus and the experimental conditions, or in other words, Re^* is not uniquely corresponding to the vapour velocity, which is one of the most important factors.

Since the experiments by Badger *et al.* were performed in an annular tube of large diameter ratio, the coefficients of heat transfer are almost unaffected by the inlet vapour velocity. The values of $(Nu_m)_{exp}$ in Fig. 6 are about five times larger than the values predicted by (31), while those of Nu^* in Fig. 7 are about ten times larger. In the latter demonstration, the discrepancy is enlarged apparently by the physical properties.

Theories concerning tubulent liquid film must

be composed on various assumptions yet. The curves inserted in Fig. 7 correspond to the theoretical results by Colburn [24], Dukler [27] and Kunz-Yeraznis [28], each of which is justified on the basis of the experimental results by Badger *et al.*, Carpenter and Goodyboontz–Dorsch respectively. The scattering of the experimental data in Figs. 7 and 8 is caused not only by the measurement errors but also by the aforementioned characteristics. It may be suggested, therefore, that the same number of theoretical curves as experimental runs must be described for exact comparison in the relation of Nu^* vs. Re^*.

6. CONCLUSIONS

The theoretical treatment of laminar filmwise condensation on a vertical surface and the comparison with experimental results hitherto reported allow following conclusions.

(1) The local and average Nusselt number are expressed by (52), (53) and (55) respectively. The effects of forced and body force convection are dominant near the leading edge and far from it respectively. The transition points of these effects are predicted approximately by (54) and (56) for the cases of local and average Nusselt number respectively.

(2) The limit values of the solutions for the cases of body force convection only and forced convection only coincide with respective similarity solutions within the accuracy of a few per cent. Of course, these possess the common nondimensional parameters of the same form respectively.

(3) The approximate solution of Shekriladze–Gomelauri coincides numerically with (52) at $RH \approx 10$. The fact that the solutions of Jacobs possess two other parameters besides those of similarity solutions, is due to the mistake of the boundary condition outside the vapour layer.

(4) For the cases where temperature differences between the vapour and the cooled surface are restricted within the limitations as shown in Table 1, experimental Nusselt number $(Nu_m)_{exp}$ agrees with $(Nu_m)_{th}$ predicted by (55) within the experimental accuracy in the range of $Nu_m < 2 \times 10^4$. In the range of $(Nu_m)_{th} > 2 \times 10^4$, however, $(Nu_m)_{exp}$ is about from 1·3 to 1·9 times as large as $(Nu_m)_{th}$. A best fitted band for the experimental results is proposed in Fig. 5. Especially for the case of very low heat flux, even though $(Nu_m)_{th} > 2 \times 10^4$, $(Nu_m)_{exp}$ agrees with $(Nu_m)_{th}$.

(5) For the cases where the temperature differences are beyond the limitations, usually for organic substances, $(Nu_m)_{exp}$ becomes larger than $(Nu_m)_{th}$ at smaller $(Nu_m)_{th}$. The cause of these larger values, together with the case of above term (4), seems due to turbulence induced in the liquid film.

(6) As to the condensation in a tube, it is inadequate to use the coordinates of condensation number Nu^* and film Reynolds number Re^* for the nondimensional demonstration of heat-transfer coefficients.

ACKNOWLEDGEMENTS

The authors acknowledge the help and participation of Mres. K. Hirata and K. Oda and Miss T. Kinugawa in the rearrangement of experimental data. Numerical computations were performed with an electronic computer FACOM 230-60 in Computer Center, Kyūshū University.

REFERENCES

1. J. C. Y. Koh, E. M. Sparrow and J. P. Hartnett, The two phase boundary layer in laminar film condensation, *Int. J. Heat Mass Transfer* **2**, 69–82 (1961).
2. J. C. Y. Koh, Film condensation in a forced-convection boundary-layer flow, *Int. J. Heat Mass Transfer* **5**, 941–954 (1962).
3. I. G. Shekriladze and V. I. Gomelauri, Theoretical study of laminar film condensation of flowing vapour, *Int. J. Heat Mass Transfer* **9**, 581–591 (1966).
4. H. R. Jacobs, An integral treatment of combined body force and forced convection in laminar film condensation, *Int. J. Heat Mass Transfer* **9**, 637–648 (1966).
5. W. Nusselt, Die Oberflächenkondensation des Wasserdampfes, *Z. Ver. Deut. Ing.* **60**, 541–580 (1916).
6. R. D. Cess, Laminar-film condensation on a flat plate in the absence of a body force, *Z. Angew. Math. Phys.* **11**, 426–433 (1960).
7. G. Poots and R. G. Milles, Effects of variable physical properties on laminar film condensation of saturated steam on a vertical flat plate, *Int. J. Heat Mass Transfer* **10**, 1677–1692 (1967).
8. A. F. Mills and R. A. Seban, The condensation coefficient of water, *Int. J. Heat Mass Transfer* **10**, 1815–1827 (1967).

9. YU. G. BUROV, Heat exchange with steam condensation on vertical tubes, *Sov. Phys. Tech. Phys.* **2**(2), 297–302 (1957).
10. G. M. HEBBARD and W. L. BADGER, Steam film heat transfer coefficients for vertical tubes, *Trans. Am. Inst. Chem. Engrs* **30**, 194–216 (1934).
11. F. L. SHEA and N. W. KRASE, Drop-wise and film condensation of steam, *Trans. Am. Inst. Chem. Engrs* **36**, 463–490 (1940).
12. J. H. GOODYKOONTZ and R. G. DORSCH, Local heat-transfer coefficients for condensation of steam in vertical down flow within a $\frac{5}{8}$-inch-diameter tube, NASA TN D-3326 (1966).
13. J. H. GOODYKOONTZ and R. G. DORSCH, Local heat-transfer coefficients and static pressures for condensation of high-velocity steam within a tube, NASA TN D-3953 (1967).
14. F. G. CARPENTER, Heat transfer and pressure drop for condensing pure vapors inside vertical tubes at high vapor velocities, Ph.D. thesis, University of Delaware (1948).
15. M. JAKOB, S. ERK and H. ECK, Verbesserte Messungen und Berechnungen des Wärmeüberganges beim Kondensieren Strömenden Dampfes in einem vertikalen Rohr, *Phys. Z.* **36**(3), 73–84 (1935).
16. *VDI-Wasserdampftafeln*. Springer, Berlin (1963).
17. *Bussei Zyōsū*, Vol. 1–7, Maruzen, Tōkyō (1963–1969).
18. *Landolt-Börnstein*, Bd, 4. Springer, Berlin (1967).
19. *International Critical Table*. McGraw-Hill, New York (1927–1930).
20. A. P. COLBURN, L. L. MILLOR and J. W. WESTWATER, Condenser–subcooler performance and design, *Trans. Am. Inst. Chem. Engrs* **38**, 447–468 (1942).
21. J. B. TEPE and A. C. MUELLER, Condensation and subcooling inside and inclined tube, *Chem. Engng Prog.* **43**(5), 267–278 (1947).
22. W. L. BADGER, C. C. MONRAD and H. W. DIAMOND, Evaporation of caustic soda to high concentrations by means of diphenyl vapors, *Ind. Engng Chem.* **22**, 700–707 (1930).
23. L. SLEGERS and R. A. SEBAN, Nusselt condensation of n-butyl alcohol, *Int. J. Heat Mass Transfer* **12**, 237–239 (1969).
24. A. P. COLBURN, Note on the calculation of condensation when a portion of the condensate layer is in turbulent motion, *Trans. Am. Inst. Chem. Engrs* **30**, 187–193 (1934).
25. E. F. CARPENTER and A. P. COLBURN, The effect of vapor velocity on condensation inside tubes, *Proc. Inst. Mech. Engrs*, London, General discussion on heat transfer, pp. 20–26 (1951).
26. C. G. KIRKBRIDE, Heat transfer by condensing vapor on vertical tube, *Trans. Am. Inst. Chem. Engrs* **30**, 170–186 (1933).
27. A. E. DUKLER, Fluid mechanics and heat transfer in vertical falling-film systems, *Chem. Engng Prog. Symp. Ser.* **56**, 1–10 (1960).
28. H. R. KUNZ and S. YERAZUNIS, An analysis of film condensation film evaporation, and single-phase heat transfer for liquid Prandtl numbers from 10^{-3} to 10^{4}, *Trans. Am. Soc. Mech. Engrs* **91**, 413–420 (1969).

CONDENSATION EN FILM LAMINAIRE SUR UNE SURFACE VERTICALE

Résumé—On résout les équations de la couche limite biphasique pour une condensation en film laminaire en utilisant une méthode approchée due à Jacobs, dans les conditions suivantes: une vapeur saturée s'écoule verticalement vers le bas, une surface refroidie à température uniforme est placée parallèlement à la direction de l'écoulement, on considère à la fois la force de volume et la convection forcée dans le film de condensat lequel est si mince que les termes d'inertie et de convection peuvent être négligés. Les résultats numériques pour les coefficients moyens de transfert thermique s'expriment par

$$Nu_m = \left\{0.656\left(1{,}20 + \frac{1}{RH}\right)^{\frac{1}{4}} Re_e^2 + 0.790\frac{Gr_e}{H}\right\}^{\frac{1}{4}}.$$

Cette expression est comparée aux résultats expérimentaux connus. L'accord est très bon dans les cas où les différences de température entre la vapeur et la surface froide sont soumises à certaines restrictions et quand Nu_m est inférieur à 2.10^4. Quand la valeur calculée de Nu_m est supérieure à 2.10^4, la valeur expérimentale de Nu_m est plus grande dans un rapport 1,3 à 1,9 sauf dans le cas d'un petit flux thermique. Hors de la restriction sur les différences de température les résultats expérimentaux relatifs aux substances organiques donnent des valeurs plus élevées que celles calculées. La cause de ces écarts semble pouvoir être rattachée à la turbulence dans le film liquide.

LAMINARE FILMKONDENSATION AN SENKRECHTEN FLÄCHEN

Zusammenfassung—Die Zwei-Phasen-Grenzschichtgleichungen für laminare Filmkondensation werden gelöst mit einer Näherungsmethode nach Jacobs unter folgenden Bedingungen: Gesättigter Dampf strömt senkrecht nach unten, eine gekühlte Oberfläche gleichmässiger Temperatur wird parallel zur Strömungsrichtung angestellt, sowohl Schwerkraft als auch erzwungene Konvektion werden im Kondensatfilm berücksichtigt, er ist so dünn, dass die Trägheits- und Konvektionsterme vernachlässigt werden können.

Numerische Ergebnisse für mittlere Wärmeübergangskoeffizienten können wie folgt dargestellt werden:

$$Nu_m = \left\{0{,}656\left(1{,}20 + \frac{1}{RH}\right)^{\frac{3}{4}} Re_1^2 + 0{,}790\,\frac{Gr_1}{H}\right\}^{\frac{1}{4}}.$$

Dieser Ausdruck wird verglichen mit den bis heute bekannten experimentallen Ergebnissen. Die Übereinstimmung ist ziemlich gut für den Fall, dass die Temperaturdifferenz zwischen Dampf und der gekühlten Oberfläche innerhalb bestimmter Grenzen liegt und dass Nu_m kleiner als $2 \cdot 10^4$ ist. Ist das vorausberechnete Nu_m grösser als $2 \cdot 10^4$, so ist das experimentelle Nu_m etwa 1,3 bis 1,9 mal grösser als das berechnete, mit Ausnahme des Falles kleiner Wärmestromdichten.

Die experimentellen Daten jenseits der Temperaturdifferenzgrenze zeigen bei organischen Substanzen höhere Werte ähnlicher Grössenordnung bei kleineren berechneten Nu_m. Der Grund für diese hohen Werte mag in der Turbulenz des Flüssigkeitsfilms zu suchen sein.

ЛАМИНАРНАЯ ПЛЕНОЧНАЯ КОНДЕНСАЦИЯ НА ВЕРТИКАЛЬНОЙ ПОВЕРХНОСТИ

Аннотация—Уравнения двухфазного пограничного слоя при ламинарной пленочной конденсации решаются с помощью приближенного метода Джэкобса при следующих условиях: насыщенный пар течет вертикально вниз; охлажденная поверхность с постоянной температурой располагается параллельно направлению потока; массовая сила и сила, возникшая за счет вынужденной конвекции, рассматриваются в настолько тонкой пленке конденсата, что инерционными и конвективными членами можно пренебречь. Численные результаты для средних коэффициентов переноса тепла выражаются следующим образом:

$$Nu_m = \left\{0{,}656\left(1{\cdot}20 + \frac{1}{RH}\right)^{4/3} Re_l^2 + 0{,}790\,\frac{Gr_l}{H}\right\}^{1/4}$$

Это выражение сравнивается с полученными ранее экспериментальными данными и соответствие между ними довольно хорошее для случаев, когда на разность температур между паром и охлажденной поверхностью накладываются определенные ограничения и Nu_m меньше 2×10^4. Когда расчетное значение Nu_m больше 2×10^4, экспериментальное значение Nu_m, приблизительно в 1,3–1,9 раза больше расчетного значения, за исключением случаев с малым подводом тепла. Экспериментальные данные без ограничений разности температуры для органических веществ показывают большие значения аналогичного порядка при меньших расчетных значениях Nu_m. Причина таких высоких значений кроется, по-видимому, в турбулентности жидкой пленки.